https://doi.org/10.5194/egusphere-2026-2831
Preprint. Discussion started: 14 July 2026

Rapid formation of gaseous benzoic sulfuric anhydride and its key role in urban-industrial sulfuric acid-ammonia nucleation

Xiaokai Guo [‡,1], Yaogeng Li [‡,1], Rui Su[1], Yanlong Yang[1], Xueping Feng[1], Guane Wang[2], Yuan Zuo[2], Rui Wang[1], Tianlei Zhang[•,1]

[1] *Shaanxi Key Laboratory of Catalysis, School of Chemical & Environment Science, Shaanxi University of Technology, Hanzhong, Shaanxi 723001, P. R. China*

[2] *Yulin Environmental Protection Engineering Co., Ltd., Yulin, Shaanxi 719000, P. R. China.*

Corresponding author: Tianlei Zhang, ztianlei88@l63.com

Abstract

Carboxylic sulfuric anhydrides are key aerosol constituents. Among these, benzoic sulfuric anhydride (BSA) has been predicted to reach up to 10^7 molecules·cm^{-3} in urban industrial regions and has been identified as a potential precursor for new particle formation (NPF). However, its formation mechanism and role in sulfuric acid-ammonia (SA-A) nucleation are unclear. Here, we employ quantum chemical (QC) calculations and atmospheric cluster dynamics simulations (ACDC) to investigate the gaseous mechanism of BSA formation and its key role in SA-A nucleation. QC calculations show that BSA forms via fast cycloaddition between BA and SO_3 (barrier of 1.5 kcal·mol^{-1}). Within 280.0-320.0 K, this route can effectively compete with the $SO_3 + (H_2O)_2$ reaction at [BA] > 10^{10} molecules·cm^{-3} and RH < 60%. ACDC simulations further reveal that at [BSA] = 10^8 molecules·cm^{-3}, the SA-A cluster formation rate increases by six orders of magnitude as temperature decreases from 298.15 K to 278.15 K. In high-BSA industrial regions (e.g., Beijing), the BSA-SA-A ternary pathway contributes 99% to total cluster formation. Notably, despite its lower concentration, BSA exhibits stronger nucleation potential than its precursor BA in the SA-A system. These findings clarify the atmospheric sources of BSA and help explain frequent NPF events in urban-industrial regions.

•Corresponding authors. Tel: +86-0916-2641083, Fax: +86-0916-2641083.
E-mail: ztianlei88@l63.com (T. L Zhang)
‡ Xiaokai Guo and Yaogeng Li contributed equally to this work.

https://doi.org/10.5194/egusphere-2026-2831
Preprint. Discussion started: 14 July 2026

1.Introduction

Atmospheric aerosols pose serious threats to human health and significantly affect global climate, radiative balance, and air quality (Zhang et al., 2012b; Heal et al., 2012; Ho et al., 2007; Lee et al., 2019; Zhao et al., 2024; Blichner et al., 2024). As a major source of atmospheric aerosols, new particle formation (NPF) arising from gas-to-particle conversion contributes approximately half of the atmospheric particle number (Gordon et al., 2017; Ma et al., 2024; Qiao et al., 2024; Liu et al., 2021b; Liu et al., 2019). Despite the atmospheric significance of NPF, field observations and chamber experiments have provided valuable information on its evolution (Lee et al., 2019; Kulmala et al., 2004). However, they cannot clarify the complex physicochemical processes governing atmospheric nucleation and particle growth (Lee et al., 2019; Kerminen et al., 2018). Therefore, molecular-scale insight into nucleation mechanisms is critical for NPF prediction, as well as for establishing theoretical support to mitigate aerosol pollution and improve air quality.

Sulfuric acid (SA), characterized by its extremely low volatility and strong acidity, has been widely recognized as a key species promoting nucleation during NPF (Almeida et al., 2013; Zhao et al., 2011; Erupe et al., 2011; Lehtipalo et al., 2016; Kulmala et al., 2013; Elm, 2021). Ammonia (A), a ubiquitous alkaline gas in the atmosphere, has been demonstrated to significantly enhance SA-driven nucleation rate (Kirkby et al., 2023; Zhang et al., 2015; Cai et al., 2023; Kirkby et al., 2011; Xie et al., 2017). However, SA-A binary nucleation alone is insufficient to account for the nucleation rates observed in the atmosphere, suggesting the involvement of additional species in the formation of critical clusters (Cai et al., 2020; Hodshire et al., 2019). In response to this, a variety of compounds have been proposed to participate in nucleation, including highly oxygenated organic molecules (HOMs) (Ortega et al., 2016; Lehtipalo et al., 2018), nitric acid (Wang et al., 2022), water (H_2O) (Zhang et al., 2012a; Kulmala et al., 2004), polyhydroxy compounds and organic acids such as pyruvic acid (Tsona Tchinda et al., 2022), lactic acid (LA) (Li et al., 2017) and glycolic acid (Perri et al., 2009; Zhang et al., 2017). These species can stabilize SA-A clusters by enhancing hydrogen bonding interactions, facilitating proton transfer and reducing cluster volatility, thereby promoting particle formation. Nevertheless, the nucleation rates predicted by current mechanisms remain than those observed in field measurements, indicating that key nucleating species and pathways have yet to be fully unidentified.

https://doi.org/10.5194/egusphere-2026-2831
Preprint. Discussion started: 14 July 2026

Carboxylic sulfuric anhydrides (CSAs) have been identified as important constituents of atmospheric organosulfur compounds (Smith et al., 2019; Mackenzie et al., 2015; Zhang et al., 2022; Rong et al., 2020; Kumar et al., 2024; Zhang et al., 2018; Wang et al., 2025). Smith et al. (2019) predicted that gaseous CSAs can reach up to 10^7 molecules·cm^{-3} in organic acid-rich environments, particularly under polluted conditions or during episodes with elevated organic acid or SO_3 concentrations. Furthermore, previous studies have shown that CSAs are formed via cycloaddition reactions between SO_3 and a variety of atmospheric organic and inorganic acids (e.g., acetic acid, oxalic acid, propionic acid, malonic acid, and iodoacetic acid) (Mackenzie et al., 2015; Kumar et al., 2024). These reactions can effectively compete with the reaction of SO_3 with water dimers $(H_2O)_2$ in acid-rich regions, implying they should be considered as an important atmospheric sink of SO_3. A representative example is the formation of acetic sulfuric anhydride from the reaction of SO_3 with acetic acid, which has been detected at both roadside and urban background sites in Leipzig. Moreover, the calculated rate coefficient for this reaction approaches the collision limit, suggesting that it can efficiently rival the $SO_3 + (H_2O)_2$ reaction in polluted regions (Kumar et al., 2024). As the simplest aromatic CSA, benzoic sulfuric anhydride (BSA) has attracted considerable attention because its concentration has been estimated to reach up to 2×10^7 molecules·cm^{-3} in potential regions characterized by elevated levels of benzoic acid (BA) and SO_3, such as Los Angeles, Azusa, Beijing and Hong Kong (Smith et al., 2019; Ho et al., 2015; Nolte et al., 1999; Ho et al., 2011). Notably, BSA has been reported to form rapidly via the reaction of BA with SO_3, with a very low energy barrier of 0.34 kcal·mol^{-1} (Zhang et al., 2023). This value is substantially lower than that of the dominant atmospheric SO_3 sink involving reaction with water dimers (5.47 kcal·mol^{-1}) (Tsona Tchinda et al., 2022). Nevertheless, the formation of BSA has not yet been kinetically compared with that of SA formation from the hydrolysis of SO_3 in regions characterized by potentially high concentrations of BA and SO_3, such as Beijing and the Pearl River Delta region (Ho et al., 2015; Ho et al., 2011). This limits an accurate and comprehensive understanding of SO_3 consumption pathways in such environments.

BSA has received considerable attention owing to its low vapor pressure, strong acidity and potentially high concentration in urban industrial regions. Previous studies have shown that BSA can form strongly bound complexes with SA/A/DMA, exhibiting substantially stronger intermolecular interactions than its precursor aromatic acid BA (Zhang et al., 2023). However, this

https://doi.org/10.5194/egusphere-2026-2831
Preprint. Discussion started: 14 July 2026

study mainly focused on intermolecular interactions, while the potential role of BSA in SA-A-driven NPF has not yet been systematically investigated. Meanwhile, increasing evidence suggests that CSAs can effectively enhance SA-A-driven ternary nucleation. For example, formic sulfuric anhydride (FSA), formed via the gas-phase reaction of formic acid (FA) with SO_3, has been reported to enhance the formation rate of SA-A clusters by more than 10^5 times in polluted urban regions such as Beijing and Tangshan (Wang et al., 2025). As one of the CSAs, BSA is expected to exert a significant promoting effect and act as an important stabilizer in SA-A-mediated NPF. Nevertheless, the specific contribution of BSA to SA-A-driven NPF has not been quantitatively characterized. This knowledge gap hinders an accurate mechanistic understanding and assessment of SA-A nucleation in the troposphere, particularly in environments characterized by high BA and SO_3 concentrations.

In this study, we first employed quantum chemical calculations combined with master equation analysis to investigate the gas-phase formation mechanism of BSA from the reaction of SO_3 with BA and to assess its atmospheric importance by comparing its rate with that of the conventional SO_3 sink pathway ($SO_3 + (H_2O)_2$). Then, the Atmospheric Cluster Dynamics Code (ACDC) is utilized to quantify the promotion effect of BSA on SA-A-drive NPF, reveal its temperature-dependent dual role in nucleation, and evaluate its contribution to cluster formation flux in typical urban industrial regions affected by fossil fuel and biomass combustion (e.g., Los Angeles). Finally, the nucleation enhancement potential of BSA is compared with its precursor BA to highlight the unique and importance role of BSA in SA-A-driven NPF, even when the atmospheric concentration of BSA is lower than that of BA. Overall, this study provides molecular-level insight into SO_3 consumption in BA-influenced environments and further improves the understanding of the role of aromatic carboxylic sulfuric anhydrides in atmospheric nucleation.

2. Computational Methods

2.1 Quantum Chemical Details. A systematic quantum chemical investigation of the gas-phase SO_3 + BA → BSA reaction was carried out using the M06-2X density functional theory (DFT) method under both anhydrous and water-assisted conditions. The M06-2X functional has been extensively validated for accurately describing noncovalent interactions and predicting thermochemical properties and equilibrium structures relevant to atmospheric

https://doi.org/10.5194/egusphere-2026-2831
Preprint. Discussion started: 14 July 2026

chemical reactions (Walker et al., 2013; Mardirossian et al., 2016; Zhao and Truhlar, 2008; Elm et al., 2012). In this work, the geometries of all species involved in the reaction were fully optimized, and harmonic vibrational frequency calculations were performed using the Gaussian 09 program (Frisch, 2009) with the 6-311G(2*d*,2*p*) basis set.

A systematic three-step configurational sampling procedure was adopted to identify the most stable geometries of $(SA)_x(A)_y(BSA)_z$ clusters within the range of $0 \le y \le x + z \le 3$. In the first step, for each cluster system, $n \times 1000$ random initial geometries ($1 \le n \le 3$) were generated with the ABCluster program (Zhang and Dolg, 2015)，followed by preliminary screening via the PM6 semiempirical approach as implemented in MOPAC 2016 (Partanen et al., 2016). Based on the PM6 screening results, the lowest-energy $n \times 100$ structures were extracted and subsequently reoptimized at the M06-2X/6-31+G(*d*,*p*) level. Finally, the energetically lowest $n \times 10$ structures were fully optimized at the M06-2X/6-311G(2*d*,2*p*) level to reliably determine the global minimum cluster configurations. Building upon the optimized geometries, high-accuracy single-point energies were calculated with the ORCA program (Neese, 2012) at the DLPNO-CCSD(T)/aug-cc-pVTZ level, yielding more reliable reaction barriers and thermodynamic parameters (Neese, 2018; Tan et al., 2022). Details of the optimized cluster structures and the corresponding Gibbs free energies are presented in the Supporting Information (Table S10 and Table S20). Metadynamics simulations were performed using the CP2K package interfaced with the PLUMED package, and detailed computational procedures are described in Part S1 of the Supporting Information. Additionally, the Multiwfn 3.8 package is employed to investigate molecular interactions (Lu and Chen, 2012; Lu, 2024; Lu and Chen, 2020; Lu and Chen, 2021).

2.2 Rate Coefficient Computations. To investigate the reaction kinetics of BA with SO_3, based on the computational methods described above, the high-pressure-limit rate coefficients were first calculated using the Variable Reaction Coordinate Variational Transition State Theory method as implemented in the Polyrate package (Meana-Pañeda et al., 2024; Zhang et al., 2024). Based on these results, temperature and pressure-dependent rate coefficients in the range of 280.0-320.0 K were subsequently obtained by solving the multi-well master equation using MESMER (Glowacki et al., 2012). In this framework, the barrierless association step from separated reactants to the pre-reactive complex was evaluated using the inverse Laplace transform method implemented in MESMER (Kumar et al., 2021), whereas the subsequent transformation from the

https://doi.org/10.5194/egusphere-2026-2831
Preprint. Discussion started: 14 July 2026

pre-reactive complex to the post-reactive complex via the transition state was treated using RRKM theory (Mallick et al., 2021; Bao et al., 2016). Tunneling effects were taken into account by applying an asymmetric Eckart tunneling model. More detailed computational information is provided in the Supporting Information (Part S2 and Part S3).

2.3 ACDC Model. The thermodynamic data derived from quantum chemical calculations at the DLPNO-CCSD(T)/aug-cc-pVTZ//M06-2X/6-311G(2*d*,2*p*) level were used as input for the Atmospheric Cluster Dynamics Code (ACDC) (McGrath et al., 2012; Zhang and Dolg, 2015) to investigate the formation rates and growth mechanisms of $(SA)_x(A)_y(BSA)_z$ clusters, with $0 \le y \le x + z \le 3$. The birth-and-death equations implemented in the ACDC model were numerically integrated using the built-in ode15s solver in MATLAB R2014a (Shampine and Reichelt, 1997), allowing for a detailed characterization of the kinetic processes governing cluster growth. The explicit form of the birth-and-death equations is given as follows:

$$\frac{dc_i}{dt} = \frac{1}{2}\sum_{j<i}\beta_{j,(i-j)}C_jC_{(i-j)} + \sum_j \gamma_{(i+j)\to i}C_{i+j} - \sum_j \beta_{i,j}C_iC_j - \frac{1}{2}\sum_{j<i}\gamma_{i\to j}C_i + Q_i - S_i \quad (1)$$

In this kinetic framework, the population density of cluster i is represented by c_i, whereas the collisional interaction rate between clusters i and j is described by $\beta_{i,j}$. The fragmentation of the larger i+j aggregate into its constituent clusters is governed by the evaporation constant $\gamma_{(i+j)\to i}$. The term Q_i represents the contribution from external formation sources. To account for removal processes, coagulation losses were incorporated using a sink coefficient of 2×10^{-2} s^{-1} (Yao et al., 2018), consistent with typical values reported for highly polluted atmospheric conditions (Liu et al., 2021a). Within the ACDC framework, boundary clusters must exhibit sufficient stability so that further growth can proceed. Therefore, the clusters $(SA)_4{\cdot}(A)_3$, $(SA)_4{\cdot}(A)_4$, and $(SA)_1{\cdot}(A)_3{\cdot}(BSA)_3$ were identified as boundary clusters.

3. Results and discussion

3.1 The gaseous mechanism of BSA formation

The electrostatic potential (ESP) mapped on the van der Waals surfaces reveals complementary charge distributions between BA and SO_3 (Fig. 1a). Specifically, the negative ESP on the O2 atom of BA (-10.55 kcal·mol^{-1}) attracts the positively charged S atom of SO_3 (+58.10 kcal·mol^{-1}), while the positive ESP on the carboxylic hydrogen of BA (+53.10 kcal·mol^{-1}) aligns with negative ESP

https://doi.org/10.5194/egusphere-2026-2831
Preprint. Discussion started: 14 July 2026

on the O3 atom of SO_3 (-12.13 kcal·mol^{-1}), indicating hydrogen bonding. This ESP complementarity supports the reaction proceeds via a cycloaddition-hydrogen abstraction mechanism. The potential energy surface of the cycloaddition reaction between SO_3 and BA was investigated at the DLPNO-CCSD(T)/aug-cc-pVTZ//M06-2X/6-311G(2*d*,2*p*) level (Fig. 1(a)). As clearly illustrated in Fig. 1(a) and Fig. S1, BA interacts with SO_3 through a strong and stable hydrogen bond (O3···H, 1.99Å, sign(λ_2)$\rho \approx$ 0.05 a.u.) and an incipient covalent interaction (S···O2, 1.65Å, sign(λ_2)$\rho \approx$ -0.09 a.u.) (Lu and Chen, 2021;Lu, 2025;Ning et al., 2024) to form a six-membered ring pre-reactive intermediate (IM), with a computed stabilization energy of 4.0 kcal·mol^{-1}. Notably, due to low ring tension, the reaction over a low energy barrier of 1.5 kcal·mol^{-1} to form BSA and the calculated Gibbs free energy (ΔG) of BSA is -4.9 kcal·mol^{-1} relative to the SO_3 + BA reactants, suggesting that this reaction is exothermic progress. Additionally, compared to cycloaddition-hydrogen abstraction between SO_3 and HCOOH, the SO_3 + BA introduction of the phenyl ring not only effectively lowers the reaction barrier but also enhances the product's stability due to the aromatic conjugation effect (Fig. S2(a)).

To further probe the bonds and structures that vary in the SO_3 + BA reactions, Metadynamics (MTD) simulations have been performed. As shown in Fig. 1(b), the reaction initially formed an SO_3···BA complex that remains stable over a certain timescale, while the S-O2 distance fluctuates around 2.5 Å, characteristic of a vdW interaction. At 1.9 ps, a six-membered-ring transition-state-like structure was observed, with the S···O2 and H···O3 distances shortening to 2.06 Å and 1.64 Å, respectively. Subsequently, at approximately 3.5 ps, the reaction clearly proceeds via a concerted mechanism, involving simultaneous hydrogen transfer from BA to the O3 atom of SO_3 and the addition of the O2 atom of BA to the S atom of SO_3, further corroborating the ESP-based predictions. The reaction then rapidly yields the BSA product, with the S-O2 and H-O3 distances stabilizing at approximately 1.75 Å and 1.00 Å, respectively, confirming the formation of new covalent bonds. Notably, BSA is formed within 4 ps, indicating a fast and efficient reaction process.

To better assess the potential importance of the SO_3 + BA reaction and its competition with the SO_3 + $(H_2O)_2$ pathway, a major sink of SO_3 in the atmosphere, the rate ratio (v_{BA}/v_{SA_wm}) was calculated over the temperature range of 280-320 K based on Eq. (2). Here, k_{BA} and k_{SA_wm} denote the rate coefficients of SO_3 + BA and SO_3 + $(H_2O)_2$ reactions, respectively, while [BA], [SO_3] and [$(H_2O)_2$] represent the corresponding species concentrations. As shown in Fig. 2, at low BA

https://doi.org/10.5194/egusphere-2026-2831
Preprint. Discussion started: 14 July 2026

concentrations (10^{10} molecules·cm^{-3}) and high relative humidity (RH ≥ 30%), v_{BA}/v_{SA_wm} remains below unity, indicating that SO_3 + $(H_2O)_2$ pathway dominates under these conditions. As BA concentration increases and RH decreases, the contribution of the SO_3 + BA pathway becomes progressively more significant. In the intermediate (blue) region ([BA] > 10^{11} molecules·cm^{-3} and RH > 40%), the two pathways are comparable, with v_{BA}/v_{SA_wm} close to 1. Notably, under conditions of high BA concentrations (> 10^{11} molecules·cm^{-3}) and low humidity (RH < 40%), the rate ratio increases markedly, reaching values up to 10, as indicated by the pink regions. This trend is consistently observed across the entire temperature range. These results indicate that the SO_3 + BA reaction can effectively compete with, or even dominate over, the SO_3 + $(H_2O)_2$ reaction under dry and polluted atmospheric conditions. Considering its advantages in both thermodynamics and kinetics, the SO_3 + BA reaction may serve as an important pathway for SO_3 consumption in environments with elevated BA concentrations, and its role should not be underestimated.

$$\frac{v_{BA}}{v_{SA\_wm}} = \frac{k_{BA}[BA][SO_3]}{k_{SA\_wm}[SO_3][(H_2O)_2]} = \frac{k_{BA}[BA]}{k_{SA\_wm}[(H_2O)_2]} \quad (2)$$

3.2 Enhancing effect of BSA in SA-A-driven NPF

This work first analysed the conformations and thermodynamic stability of $(SA)_x(A)_y(BSA)_z$ ($0 \le y \le x + z \le 3$) clusters. It then investigated the influence of BSA on SA-A nucleation and the effects of temperature and precursor concentrations. Finally, the formation rates and enhancement factors for BSA and its precursor BA were compared.

3.2.1 Cluster Structures and stability analysis

The stable conformers of ternary $(SA)_x(A)_y(BSA)_z$ ($1 \le x$, $1 \le y$, $x + z \le 3$, $1 \le z \le 2$) clusters are shown in Fig. 2. As the number of molecules increases, the cluster structures gradually transition from ring to cage configuration. BSA can interact with the SA-A system via hydrogen bonding and proton transfer, leading to the formation of comparatively stable clusters. Notably, in clusters where x > y protons transfer solely from SA to A without BSA involvement, whereas in $x \le y$ clusters, such as $(SA)_1·(A)_2·(BSA)_1$, $(SA)_1·(A)_2·(BSA)_2$, $(SA)_2·(A)_3·(BSA)_1$, and $(SA)_1·(A)_3·(BSA)_2$, excess A accepts protons directly from BSA. This is attributed to the stronger acidity of SA (pKa = -3.0) compared to BSA (pKa = -2.3). Interestingly, the addition of BSA promotes more complete proton transfer within the SA-A clusters. For example, proton transfer does not occur in pure SA·A cluster (Fig.S7(a)). In SA·A·BSA (Fig.S7(b)), complete proton transfer from SA to A proton transfer yields

https://doi.org/10.5194/egusphere-2026-2831
Preprint. Discussion started: 14 July 2026

a new H1-N bond with an LBO of 0.668 a.u., which rises to 0.695 a.u. in SA·A·$(BSA)_2$ (Fig.S7(c)), underscoring the promotive role of BSA. In conclusion, BSA plays a significant role in forming relatively stable clusters with SA-A system through interactions by hydrogen bond and proton-transfer.

Based on the above cluster structures analysis, the ΔG (kcal·mol^{-1}, Table S9) and the total evaporation rate ($\Sigma\gamma$, s^{-1}, Table S12) were calculated at five different temperatures (T = 298.15, 288.15, 278.15, 268.15, and 258.15 K) to evaluate cluster stability. The results demonstrate that incorporating BSA significantly improves the stability of the SA-A system across all studied temperatures. For instance, at 278.15 K, the formation of $(SA)_1\cdot(A)_1\cdot(BSA)_1$ from $(SA)_1\cdot(A)_1$ leads to a decrease in ΔG to -17.13 kcal·mol^{-1}, and a similar trend is observed for $(SA)_2\cdot(A)_1\cdot(BSA)_1$, $(SA)_2\cdot(A)_2\cdot(BSA)_1$ and $(SA)_2\cdot(A)_3\cdot(BSA)_1$. Notably, the ΔG value for $(SA)_1\cdot(A)_3\cdot(BSA)_2$ (-56.93 kcal·mol^{-1}) was slightly lower than that of the most stable binary cluster $(SA)_3\cdot(A)_3$ (-55.04 kcal·mol^{-1}). Kinetically, the $\Sigma\gamma$ of $(SA)_1\cdot(A)_1\cdot(BSA)_1$ (5.96×10^0 s^{-1}) was about 4 orders of magnitude lower than that of the binary cluster $(SA)_1\cdot(A)_1$ (4.19×10^4 s^{-1}). Similarly, the $\Sigma\gamma$ of $(SA)_1\cdot(A)_3\cdot(BSA)_2$ (1.45×10^{-1} s^{-1}) was approximately 10 times lower than $(SA)_3\cdot(A)_3$ (9.82×10^0 s^{-1}). Accordingly, ΔG and $\Sigma\gamma$ demonstrates that BSA addition enhances the stability of SA-A clusters.

3.2.2 The cluster formation rates on the BSA-SA-A system

To elucidate how BSA affects the kinetic process, a series of ACDC simulations under varying temperatures and monomer concentrations ([SA] = 10^6-10^8, [A] = 10^7-10^{11} and [BSA] = 10^5-10^8 molecules·cm^{-3}). Fig. 3(a) illustrates the influence of BSA on J at different temperatures (298.15, 288.15, 278.15, 268.15, and 258.15 K) with the median concentration of A (10^9 molecules·cm^{-3}) and SA (10^7 molecules·cm^{-3}). The results show that J increase rapidly with decreasing temperature and rising [BSA]. Specifically, at a high [BSA] of 10^8 molecules·cm^{-3}, J increases by approximately 6 orders of magnitude as the temperature decreases from 298.15 K to 278.15 K. This behavior is primarily attributed to the thermodynamically favorable stabilization of BSA-SA-A clusters at lower temperatures. Moreover, J increases significantly with rising [BSA] concentration, especially when [BSA] exceeds 10^6 molecules·cm^{-3}. At 258.15 K, as [BSA] increases from 10^6 to 10^8 molecules·cm^{-3}, J increased from 4.87×10^{-3} $cm^{-3}s^{-1}$ to 2.21×10^1 $cm^{-3}s^{-1}$.

Besides temperature and [BSA], the concentration of the SA and A was another important factor influencing the J. As shown in Fig. 3(b), a pronounced positive correlation was observed

https://doi.org/10.5194/egusphere-2026-2831
Preprint. Discussion started: 14 July 2026

between J and [A]. With J increasing by approximately 11 orders of magnitude as [A] rises from 10^7 to 10^{11} molecules·cm^{-3}. Similarly, J increases with [SA] over the range of 10^6 to 10^8 molecules·cm^{-3}, reaching 5.08×10^2 cm^{-3}s^{-1} at higher [A] (10^{11} molecules·cm^{-3}). The enhancement in nucleation is mainly attributed to the increased concentration of nucleation precursors, which leads to an increase in the number of SA-A-BSA clusters. Overall, these findings clearly demonstrate that BSA participation strongly enhances J in SA-A-driven NPF, especially at low temperatures, high [BSA], and higher concentrations of nucleation precursors (SA and A).

3.3.3 Cluster formation pathways

To further elucidate the role of BSA in the BSA-SA-A system, the dominant cluster growth paths of clusters were traced. As shown in Fig. 4(a), the major growth routes at 278.15 K under conditions of CS = 0.02 s^{-1}, [SA] = 10^7 molecules·cm^{-3}, [A] = 10^9 molecules·cm^{-3}, and [BSA] = 5×10^6 molecules·cm^{-3} can be broadly classified into two categories. The dominant pathways of clusters growing out of BSA-SA-A system can be divided into two paths. The first pathway corresponds to the pure SA-A-based clustering route, indicated by the blue arrows. In this pathway, cluster growth is initiated by the formation of the $(SA)_2$ dimer, followed by sequential collisions with SA monomers, A monomers, or acid-base pairs. These processes preferentially generate clusters containing equal numbers of acid and base molecules, ultimately leading to the formation of the stable $(SA)_3(A)_3$, which eventually exits the system with a contribution ratio of 6%. In addition to the pure SA-A pathway, a distinct BSA-involved growth mechanism is observed, in which BSA serves dual functions as a "catalyst" and a direct "participant" in cluster growth. When BSA acting as a "catalyst", BSA transiently stabilizes intermediate clusters without remaining in the final products. Specifically, the $(SA)_2{\cdot}(A)_2{\cdot}$BSA cluster first collides with an SA monomer to form $(SA)_3{\cdot}(A)_2{\cdot}$BSA cluster, after which BSA readily evaporates, yielding the stable $(SA)_3{\cdot}(A)_2$ cluster with a proportion of 11%. Meanwhile, when BSA acts as a "participant". The pathway starts with the complete collision (100%) of one molecule A with BSA to form a dimer A·BSA. Then, the SA·A·BSA cluster can be formed via two pathways: (*i*) the combination of the A·BSA cluster with a single SA monomer with the proportion of 91% and (*ii*) cluster SA·A with the BSA monomer with a proportion of 7%. The SA·A·BSA cluster can further react with the A molecule to form $SA{\cdot}(A)_2{\cdot}$BSA with a branching ratio of 59%. Two different pathways for the formation of the larger $SA{\cdot}(A)_2{\cdot}(BSA)_2$ cluster; one is the collision reaction between the $(A)_2{\cdot}(BSA)_2$ cluster and a single

https://doi.org/10.5194/egusphere-2026-2831
Preprint. Discussion started: 14 July 2026

SA monomer with a proportion of 54%. The other is the collision between the SA·$(A)_2$·BSA cluster and a single BSA monomer with a proportion of 39%. The SA·$(A)_2$·$(BSA)_2$ cluster will collide with A molecule, forming SA·$(A)_3$·$(BSA)_2$, which ultimately grows out of the system with a dominant contribution ratio of 94%. The dual roles of BSA in SA-A clusters are also observed at lower temperatures of 268.15 K and 258.15 K; however, at elevated temperatures (288.15 K and 298.15 K), the BSA-involved pathway is simplified due to increased evaporation rates, with BSA exhibiting only the role of a "participant" (as shown in Fig. S8-S11).

As discussed above, a comprehensive understanding of the BSA-promoted SA-A nucleation mechanism requires further evaluation of how environmental parameters, including temperature and precursor concentrations ([BSA], [SA] and [A]), influence the relative contributions of different cluster growth pathways. Among these factors, temperature variation has a relatively weak effect on pathway branching: over 258.15-298.15 K, while higher temperatures slightly enhance the share of the pure SA-A binary pathway, the BSA-involved route remains dominant (generally > 80%) (Fig. 5(b)). Under typical environmental conditions, the importance of the BSA-involved route increases markedly with increasing [BSA] (Fig. 5(c)). In regions with low [BSA], such as western coastal Bay of Bengal (Boreddy et al., 2017), BSA contributes only marginally to SA-A cluster growth. However, in polluted urban industrial regions, where elevated BSA concentrations can arise from fossil-fuel combustion and biomass burning emissions, the BSA-mediated pathway becomes increasingly dominant. The contribution of the BSA-involved pathway also shows a clear negative correlated with [SA] (Fig. 5(d)). Specifically, in regions with low sulfuric acid concentrations, such as Beijing (3.0×10^6 molecules·cm^{-3}) (Lu et al., 2019), Nanjing (1.85×10^6 molecules·cm^{-3}) (Yang et al., 2021) and Atlanta (2.5×10^6 molecules·cm^{-3}) (McMurry et al., 2005), the BSA-involved pathway contributes 100% and plays a dominant role. In contrast, in regions with high sulfuric acid concentrations, the contribution rate is only 6%. The SA-A-BSA ternary pathway dominates (93-94%) when [A] ranges from 10^7 to 10^{10} molecules·cm^{-3}, while an increase in [A] to 10^{11} molecules·cm^{-3} reduces the ternary pathway's share to 84% and raises the binary pathway's to 16% (Fig. 5(e)). However, the ternary nucleation pathway still plays a dominant role. This phenomenon indicates that even in ammonia-polluted coastal regions such as Zhejiang ([NH_3] ≈10^4 pptv) (Zheng et al., 2015), the BSA-involved SA-A nucleation pathway remains the dominant contributor to NPF.

Overall, BSA significantly promotes SA-A nucleation primarily in regions with high [BSA]

https://doi.org/10.5194/egusphere-2026-2831
Preprint. Discussion started: 14 July 2026

and low [SA] levels, such as urban industrial areas (e.g., Los Angeles, Azusa and Yufa) and certain low-[SA] environments (e.g., Beijing, Shanghai, and Atlanta), while its effect is limited in regions with low BSA or high sulfuric acid concentrations.

3.3 Comparison of the Enhancement Effects of BSA and BA on the SA-A System

To evaluate the enhancement potential of BSA and its precursor BA in the SA-A-driven NPF process, the ΔG of relevant clusters were analyzed. A comparison of ΔG values for $(BSA)_x(SA)_y(A)_3$ (green histogram) and $(BA)_x(SA)_y(A)_3$ (blue histogram) clusters (x = 0-3, x + y = 3) at 278.15 K is presented in Fig. 7(a). The binary $(SA)_3(A)_3$ cluster, which represents the most stable configuration in the SA-A system, is included for reference. A clear difference in thermodynamic stability is observed between the BA-containing and BSA-containing clusters. Specifically, for all investigated $(BA)_{1\text{-}3}(SA)_{0\text{-}2}(A)_3$ clusters, the ΔG values are substantially less negative than that of the reference $(SA)_3(A)_3$ cluster, with energy differences ranging from 18.8 to 49.75 kcal·mol^{-1}. In contrast, the ΔG values of the $(BSA)_{1\text{-}3}(SA)_{0\text{-}2}(A)_3$ clusters are much closer to those of the $(SA)_3(A)_3$ reference cluster, with differences in the range of 1.53-10.41 kcal·mol^{-1}. More importantly, the $(BSA)_1(SA)_2(A)_3$ cluster exhibits a more negative ΔG value than the $(SA)_3(A)_3$ cluster. These results indicate that the addition of BSA contributes more favorably than BA to cluster stability in the SA-A system. The enhanced stabilizing effect of BSA is mainly attributed to its stronger intermolecular interactions with SA-A clusters, which facilitate the formation of more thermodynamically favorable cluster configurations.

Based on the thermodynamic analysis, the corresponding J and enhancement strength (R) in the BSA-SA-A and BA-SA-A systems were investigated and compared in Fig. 7(b). For the BA-containing system, the calculated particle formation rate remains extremely low across the investigated concentration range. Even when the BA concentration increases to 10^{10} molecules·cm^{-3}, the $J_{BA\text{-}SA\text{-}A}$ at 278.15 K is only 1.29×10^{-8} cm^{-3}s^{-1}, indicating that BA contributes negligibly to SA-A cluster formation. In contrast, the incorporation of BSA leads to a dramatic enhancement in nucleation activity. Although [BSA] being two orders of magnitude less concentrated than [BA], increasing [BSA] to 10^7 molecules·cm^{-3} results in a $J_{BSA\text{-}SA\text{-}A}$ value that exceeds that of the BA-containing system by nearly six orders of magnitude. Correspondingly, the $R_{BSA\text{-}SA\text{-}A}$ reaches a value of 83 at [BSA] is 10^7 molecules·cm^{-3}, whereas R is only 1 in the BA-SA-A system even when [BA] is 10^{10} molecules·cm^{-3}. The substantial increase in J for the BSA-SA-A system can be attributed to

https://doi.org/10.5194/egusphere-2026-2831
Preprint. Discussion started: 14 July 2026

the favorable ΔG of the $(SA)_x(A)_y(BSA)_z$ clusters. In contrast, the relatively unfavorable ΔG constrains cluster formation in the BA-SA-A system, even under high BA concentrations. These results further confirm that BSA effectively promotes the formation of the SA-A-driven NPF.

4. Summary and Conclusions

In this work, quantum chemical (QC) calculations, master equation analysis and ACDC kinetic modeling were combined to investigate gas-phase BSA formation and its role in SA-A nucleation.

QC calculations show that BSA formation via the SO_3 + BA reaction has a low energy barrier of 1.5 kcal·mol^{-1} and is exothermic by 4.9 kcal·mol^{-1}. Within the temperature range of 280.0-320.0 K, under high BA concentrations (> 10^{11} molecules·cm^{-3}) and low relative humidity (< 40% RH), the rate ratio (ν_{BA}/ν_{SA_wm}) between the SO_3 + BA pathway and the SO_3 + $(H_2O)_2$ pathway reaches 10. Consequently, the SO_3 + BA pathway is both kinetically and thermodynamically favorable, making it an important sink for SO_3 in polluted regions with elevated BA levels and dry conditions.

Cluster structure analysis reveals that BSA incorporation into SA-A clusters increases the number of hydrogen bonds and facilitates proton transfer, driving the structural transition from ring to cage configurations, thereby enhancing cluster stability and reducing ΔG by 17.13-55.04 kcal·mol^{-1} at 278.15 K. ACDC kinetic simulations further show that when [BSA] exceeds 10^6 molecules·cm^{-3}, the cluster formation rate (J) increases by 1-4 orders of magnitude, while at [BSA] = 10^8 molecules·cm^{-3}, J increases by approximately 10^6-fold as temperature decreases from 298.15 K to 278.15 K. Under cold and polluted urban conditions with elevated BSA levels (e.g., Los Angeles and Beijing), BSA acts as both a catalyst and a direct participant, with BSA-involved pathways contributing up to 99% of the total cluster formation flux.

Comparative analysis demonstrates that BSA promotes SA-A nucleation more efficiently than its precursor BA. BSA-containing clusters exhibit significantly more favorable ΔG values than those containing BA, even surpassing the most stable binary SA-A clusters, whereas BA hardly improves cluster thermodynamic stability. Although the observed BA concentration in urban industrial areas such as Los Angeles and Beijing is approximately 10^{10} molecules·cm^{-3}, about two orders of magnitude higher than the predicted BSA concentration, the BSA-SA-A system still yields J values approximately six orders of magnitude higher than those of the BA-SA-A system. These findings indicate that BSA serves as a more effective nucleation precursor than BA because of its superior

https://doi.org/10.5194/egusphere-2026-2831
Preprint. Discussion started: 14 July 2026

ability to stabilize molecular clusters and plays a crucial role in promoting SA-A-driven NPF in typical urban-industrial areas, including Beijing, Shanghai, and Azusa.

In summary, BSA forms rapidly in the gas phase and critically promotes SA-A-driven NPF, especially in urban industrial regions affected by fossil fuel and biomass combustion. These findings identify BSA as a previously unrecognized yet highly efficient sulfur-containing nucleation precursor that effectively stabilizes molecular clusters during atmospheric nucleation, providing new mechanistic insights into sulfur-driven aerosol formation and the frequent high-NPF events observed in polluted urban environments.

Data availability

All data underlying this study can be obtained from the corresponding author upon reasonable request.

Author contributions

XG: Responsible for research design and methodological development, conducted experimental investigations, participated in funding acquisition, and drafted the original manuscript. YL: Contributed to manuscript writing and revision (review), data curation, methodological support, and experimental work.RS: Responsible for manuscript review and data curation. YY: Mainly involved in data curation and visualization analysis. XF: Responsible for manuscript editing and data curation. GW: Contributed to data curation and manuscript review and revision. YZ: Participated in methodological design and manuscript review and revision. RW: Responsibility was taken for data curation and project administration. TZ: responsible for manuscript review and editing, and also participated in funding acquisition.

Competing interests

The contact author has declared that none of the authors has any competing interests.

Acknowledgments

This work was supported by the National Natural Science Foundation of China (No: 22203052; 22073059)，and Yulin Science and Technology Light Talent Program (No:KJZG-2025-K+G-09).

Financial support.

The research has been supported by the National Natural Science Foundation of China (No:

https://doi.org/10.5194/egusphere-2026-2831
Preprint. Discussion started: 14 July 2026

22203052; 22073059)，and Yulin Science and Technology Light Talent Program (No:KJZG-2025-K+G-09).

References

Almeida, J., Schobesberger, S., Kürten, A., Ortega, I. K., Kupiainen-Määttä, O., Praplan, A. P., Adamov, A., Amorim, A., Bianchi, F., Breitenlechner, M., David, A., Dommen, J., Donahue, N. M., Downard, A., Dunne, E., Duplissy, J., Ehrhart, S., Flagan, R. C., Franchin, A., Guida, R., Hakala, J., Hansel, A., Heinritzi, M., Henschel, H., Jokinen, T., Junninen, H., Kajos, M., Kangasluoma, J., Keskinen, H., Kupc, A., Kurtén, T., Kvashin, A. N., Laaksonen, A., Lehtipalo, K., Leiminger, M., Leppä, J., Loukonen, V., Makhmutov, V., Mathot, S., McGrath, M. J., Nieminen, T., Olenius, T., Onnela, A., Petäjä, T., Riccobono, F., Riipinen, I., Rissanen, M., Rondo, L., Ruuskanen, T., Santos, F. D., Sarnela, N., Schallhart, S., Schnitzhofer, R., Seinfeld, J. H., Simon, M., Sipilä, M., Stozhkov, Y., Stratmann, F., Tomé, A., Tröstl, J., Tsagkogeorgas, G., Vaattovaara, P., Viisanen, Y., Virtanen, A., Vrtala, A., Wagner, P. E., Weingartner, E., Wex, H., Williamson, C., Wimmer, D., Ye, P., Yli-Juuti, T., Carslaw, K. S., Kulmala, M., Curtius, J., Baltensperger, U., Worsnop, D. R., Vehkamäki, H., and Kirkby, J.: Molecular understanding of sulphuric acid-amine particle nucleation in the atmosphere, Nature, https://doi.org/10.1038/nature12663, 2013.

Bao, J. L., Zhang, X., and Truhlar, D. G.: Barrierless association of CF_2 and dissociation of C_2F_4 by variational transition-state theory and system-specific quantum Rice-Ramsperger-Kassel theory, P. Natl. Acad. Sci., 113, 13606-13611, https://doi.org/10.1073/pnas.1616208113, 2016.

Blichner, S. M., Yli-Juuti, T., Mielonen, T., Pöhlker, C., Holopainen, E., Heikkinen, L., Mohr, C., Artaxo, P., Carbone, S., Meller, B. B., Quaresma Dias-Júnior, C., Kulmala, M., Petäjä, T., Scott, C. E., Svenhag, C., Nieradzik, L., Sporre, M., Partridge, D. G., Tovazzi, E., Virtanen, A., Kokkola, H., and Riipinen, I.: Process-evaluation of forest aerosol-cloud-climate feedback shows clear evidence from observations and large uncertainty in models, Nat. Commun., 15, 969, https://doi.org/10.1038/s41467-024-45001-y, 2024a.

Boreddy, S. K., Mochizuki, T., Kawamura, K., Bikkina, S., and Sarin, M. J. A. E.: Homologous series of low molecular weight (C1-C10) monocarboxylic acids, benzoic acid and hydroxyacids in fine-mode ($PM_{2.5}$) aerosols over the Bay of Bengal: Influence of heterogeneity in air masses and formation pathways, Atmos. Environ., 167, 170-180, https://doi.org/10.1016/j.atmosenv.2017.08.008, 2017.

Cai, R., Yan, C., Yang, D., Yin, R., Lu, Y., Deng, C., Fu, Y., Ruan, J., Li, X., Kontkanen, J., Zhang, Q., Kangasluoma, J., Ma, Y., Hao, J., Worsnop, D. R., Bianchi, F., Paasonen, P., Kerminen, V. M., Liu, Y., Wang, L., Zheng, J., Kulmala, M., and Jiang, J.: Sulfuric acid-amine nucleation in urban Beijing, Atmos. Chem. Phys., 21, 2457-2468, https://doi.org/10.5194/acp-21-2457-2021, 2021.

Cai, R., Yin, R., Li, X., Xie, H. B., Yang, D., Kerminen, V. M., Smith, J. N., Ma, Y., Hao, J., Chen, J., Kulmala, M., Zheng, J., Jiang, J., and Elm, J.: Significant contributions of trimethylamine to sulfuric acid nucleation in polluted environments, npj Clim. Atmos. Sci., 6, 75, https://doi.org/10.1038/s41612-023-00405-3, 2023a

Elm, J., Bilde, M., and Mikkelsen, K. V.: Assessment of density functional theory in predicting structures and free energies of reaction of atmospheric prenucleation clusters, J. Chem. Theory Comput., 8, 2071-2077, https://doi.org/10.1021/ct300192p, 2012.

Elm, J. J. A. o.: Clusteromics I: Principles, Protocols, and applications to sulfuric acid-base cluster formation, ACS Omega., 6, 7804-7814, https://doi.org/10.1021/acsomega.1c00306, 2021.

https://doi.org/10.5194/egusphere-2026-2831
Preprint. Discussion started: 14 July 2026

Erupe, M. E., Viggiano, A. A., and Lee, S. H.: The effect of trimethylamine on atmospheric nucleation involving H2SO4, Atmos. Chem. Phys., 11, https://doi.org/10.5194/acp-11-4767-2011, 2011.

Frisch, M. J., Trucks, G. W., Schlegel, H. B., Scuseria, G. E., Robb, M. A., Cheeseman, J. R., Scalmani, G., Barone, V., Mennucci, B., Petersson, G. A., Nakatsuji, H., Caricato, M., Li, X., Hratchian, H. P., Izmaylov, A. F., Bloino, J., Zheng, G., Sonnenberg, J. L., Hada, M., Ehara, M., Toyota, K., Fukuda, R., Hasegawa, J., Ishida, M., Nakajima, T., Honda, Y., Kitao, O., Nakai, H., Vreven, T., Montgomery, J. A., Jr., Peralta, J. E., Ogliaro, F., Bearpark, M., Heyd, J. J., Brothers, E., Kudin, K. N., Staroverov, V. N., Kobayashi, R., Normand, J., Raghavachari, K., Rendell, A., Burant, J. C., Iyengar, S. S., Tomasi, J., Cossi, M., Rega, N., Millam, J. M., Klene, M., Knox, J. E., Cross, J. B., Bakken, V., Adamo, C., Jaramillo, J., Gomperts, R., Stratmann, R. E., Yazyev, O., Austin, A. J., Cammi, R., Pomelli, C., Ochterski, J. W., Martin, R. L., Morokuma, K., Zakrzewski, V. G., Voth, G. A., Salvador, P., Dannenberg, J. J., Dapprich, S., Daniels, A. D., Farkas, Ö., Foresman, J. B., Ortiz, J. V., Cioslowski, J., and Fox, D. J Gaussian09 Revision D. 01, Gaussian Inc. Wallingford CT, http://www.gaussian. com (last access: 1 May 2024), 2009.

Glowacki, D. R., Liang, C.-H., Morley, C., Pilling, M. J., and Robertson, S. H.: MESMER: an open-source master equation solver for multi-energy well reactions, J. Phys. Chem. A, 116, 9545-9560, https://doi.org/10.1021/jp3051033, 2012.

Gordon, H., Kirkby, J., Baltensperger, U., Bianchi, F., Breitenlechner, M., Curtius, J., Dias, A., Dommen, J., Donahue, N. M., Dunne, E. M., Duplissy, J., Ehrhart, S., Flagan, R. C., Frege, C., Fuchs, C., Hansel, A., Hoyle, C. R., Kulmala, M., Kürten, A., Lehtipalo, K., Makhmutov, V., Molteni, U., Rissanen, M. P., Stozkhov, Y., Tröstl, J., Tsagkogeorgas, G., Wagner, R., Williamson, C., Wimmer, D., Winkler, P. M., Yan, C., and Carslaw, K. S.: Causes and importance of new particle formation in the present-day and preindustrial atmospheres, J. Geophys. Res. Atmos., 122, 8739-8760, https://doi.org/10.1002/2017JD026844, 2017.

Heal, M. R., Kumar, P., and Harrison, R. M.: Particles, air quality, policy and health, Chem. Soc. Rev., 41, 6606-6630, https://doi.org/10.1039/C2CS35076A, 2012.

Ho, K. F., Cao, J. J., Lee, S. C., Kawamura, K., Zhang, R. J., Chow, J. C., and Watson, J. G.: Dicarboxylic acids, ketocarboxylic acids, and dicarbonyls in the urban atmosphere of China, J. Geophys. Res. Atmos., 112, https://doi.org/10.1029/2006JD008011, 2007.

Ho, K. F., Ho, S. S. H., Lee, S. C., Kawamura, K., Zou, S. C., Cao, J. J., and Xu, H. M.: Summer and winter variations of dicarboxylic acids, fatty acids and benzoic acid in $PM_{2.5}$ in Pearl Delta River Region, China, Atmos. Chem. Phys., 11, https://doi.org/10.5194/acp-11-2197-2011, 2197-2208, 2011.

Ho, K. F., Huang, R. J., Kawamura, K., Tachibana, E., Lee, S. C., Ho, S. S. H., Zhu, T., and Tian, L.: Dicarboxylic acids, ketocarboxylic acids, α-dicarbonyls, fatty acids and benzoic acid in PM2.5 aerosol collected during CAREBeijing-2007: an effect of traffic restriction on air quality, Atmos. Chem. Phys., 15, 3111-3123, https://doi.org/10.5194/acp-15-3111-2015, 2015.

Hodshire, A. L., Campuzano-Jost, P., Kodros, J. K., Croft, B., Nault, B. A., Schroder, J. C., Jimenez, J. L., and Pierce, J. R.: The potential role of methanesulfonic acid (MSA) in aerosol formation and growth and the associated radiative forcings, Atmos. Chem. Phys., 19, 3137-3160, https://doi.org/10.5194/acp-19-3137-2019, 2019.

Kerminen, V. M., Chen, X., Vakkari, V., Petäjä, T., Kulmala, M., and Bianchi, F.: Atmospheric new particle formation and growth: review of field observations, Environ. Chem. Lett., 13, 103003, https://doi.org/10.1088/1748-9326/aadf3c, 2018.

https://doi.org/10.5194/egusphere-2026-2831
Preprint. Discussion started: 14 July 2026

Kirkby, J., Curtius, J., Almeida, J., Dunne, E., Duplissy, J., Ehrhart, S., Franchin, A., Gagné, S., Ickes, L., Kürten, A., Kupc, A., Metzger, A., Riccobono, F., Rondo, L., Schobesberger, S., Tsagkogeorgas, G., Wimmer, D., Amorim, A., Bianchi, F., Breitenlechner, M., David, A., Dommen, J., Downard, A., Ehn, M., Flagan, R. C., Haider, S., Hansel, A., Hauser, D., Jud, W., Junninen, H., Kreissl, F., Kvashin, A., Laaksonen, A., Lehtipalo, K., Lima, J., Lovejoy, E. R., Makhmutov, V., Mathot, S., Mikkilä, J., Minginette, P., Mogo, S., Nieminen, T., Onnela, A., Pereira, P., Petäjä, T., Schnitzhofer, R., Seinfeld, J. H., Sipilä, M., Stozhkov, Y., Stratmann, F., Tomé, A., Vanhanen, J., Viisanen, Y., Vrtala, A., Wagner, P. E., Walther, H., Weingartner, E., Wex, H., Winkler, P. M., Carslaw, K. S., Worsnop, D. R., Baltensperger, U., and Kulmala, M.: Role of sulphuric acid, ammonia and galactic cosmic rays in atmospheric aerosol nucleation, Nature, 476, https://doi.org/10.1038/nature10343, 2011.

Kirkby, J., Amorim, A., Baltensperger, U., Carslaw, K. S., Christoudias, T., Curtius, J., Donahue, N. M., Haddad, I. E., Flagan, R. C., Gordon, H., Hansel, A., Harder, H., Junninen, H., Kulmala, M., Kürten, A., Laaksonen, A., Lehtipalo, K., Lelieveld, J., Möhler, O., Riipinen, I., Stratmann, F., Tomé, A., Virtanen, A., Volkamer, R., Winkler, P. M., and Worsnop, D. R.: Atmospheric new particle formation from the CERN CLOUD experiment, Nat. Geosci., 16, 948-957, https://doi.org/10.1038/s41561-023-01305-0, 2023.

Kulmala, M., Vehkamäki, H., Petäjä, T., Dal Maso, M., Lauri, A., Kerminen, V. M., Birmili, W., and McMurry, P. H.: Formation and growth rates of ultrafine atmospheric particles: a review of observations, J. Aerosol Sci., 35, 143-176, https://doi.org/10.1016/j.jaerosci.2003.10.003, 2004.

Kulmala, M., Kontkanen, J., Junninen, H., Lehtipalo, K., Manninen, H. E., Nieminen, T., Petäjä, T., Sipilä, M., Schobesberger, S., Rantala, P., Franchin, A., Jokinen, T., Järvinen, E., Äijälä, M., Kangasluoma, J., Hakala, J., Aalto, P. P., Paasonen, P., Mikkilä, J., Vanhanen, J., Aalto, J., Hakola, H., Makkonen, U., Ruuskanen, T., Mauldin, R. L., Duplissy, J., Vehkamäki, H., Bäck, J., Kortelainen, A., Riipinen, I., Kurtén, T., Johnston, M. V., Smith, J. N., Ehn, M., Mentel, T. F., Lehtinen, K. E. J., Laaksonen, A., Kerminen, V.-M., and Worsnop, D. R.: Direct Observations of Atmospheric Aerosol Nucleation, Science, 339, 943-946, https://doi.org/10.1126/science.1227385, 2013.

Kumar, A., Iyer, S., Barua, S., Brean, J., Besic, E., Seal, P., Dall'Osto, M., Beddows, D. C. S., Sarnela, N., Jokinen, T., Sipilä, M., Harrison, R. M., and Rissanen, M.: Direct Measurements of Covalently Bonded Sulfuric Anhydrides from Gas-Phase Reactions of SO_3 with Acids under Ambient Conditions, J. Am. Chem. Soc., 146, 15562-15575, https://doi.org/10.1021/jacs.4c04531, 2024.

Lee, S. H., Gordon, H., Yu, H., Lehtipalo, K., Haley, R., Li, Y., and Zhang, R.: New Particle Formation in the Atmosphere: From Molecular Clusters to Global Climate, J. Geophys. Res. Atmos., 124, 7098-7146, https://doi.org/10.1029/2018JD029356, 2019.

Lehtipalo, K., Rondo, L., Kontkanen, J., Schobesberger, S., Jokinen, T., Sarnela, N., Kürten, A., Ehrhart, S., Franchin, A., Nieminen, T., Riccobono, F., Sipilä, M., Yli Juuti, T., Duplissy, J., Adamov, A., Ahlm, L., Almeida, J., Amorim, A., Bianchi, F., Breitenlechner, M., Dommen, J., Downard, A. J., Dunne, E. M., Flagan, R. C., Guida, R., Hakala, J., Hansel, A., Jud, W., Kangasluoma, J., Kerminen, V. M., Keskinen, H., Kim, J., Kirkby, J., Kupc, A., Kupiainen-Määttä, O., Laaksonen, A., Lawler, M. J., Leiminger, M., Mathot, S., Olenius, T., Ortega, I. K., Onnela, A., Petäjä, T., Praplan, A., Rissanen, M. P., Ruuskanen, T., Santos, F. D., Schallhart, S., Schnitzhofer, R., Simon, M., Smith, J. N., Tröstl, J., Tsagkogeorgas, G., Tomé, A., Vaattovaara, P., Vehkamäki, H., Vrtala, A. E., Wagner, P. E., Williamson, C., Wimmer, D., Winkler, P. M., Virtanen, A., Donahue, N. M., Carslaw, K. S., Baltensperger, U., Riipinen, I., Curtius, J., Worsnop, D. R., and Kulmala, M.: The effect of acid–

https://doi.org/10.5194/egusphere-2026-2831
Preprint. Discussion started: 14 July 2026

base clustering and ions on the growth of atmospheric nano-particles, Nat. Commun., 7, 11594, https://doi.org/10.1038/ncomms11594, 2016.

Lehtipalo, K., Yan, C., Dada, L., Bianchi, F., Xiao, M., Wagner, R., Stolzenburg, D., Ahonen, L. R., Amorim, A., Baccarini, A., Bauer, P. S., Baumgartner, B., Bergen, A., Bernhammer, A. K., Breitenlechner, M., Brilke, S., Buchholz, A., Mazon, S. B., Chen, D., Chen, X., Dias, A., Dommen, J., Draper, D. C., Duplissy, J., Ehn, M., Finkenzeller, H., Fischer, L., Frege, C., Fuchs, C., Garmash, O., Gordon, H., Hakala, J., He, X., Heikkinen, L., Heinritzi, M., Helm, J. C., Hofbauer, V., Hoyle, C. R., Jokinen, T., Kangasluoma, J., Kerminen, V. M., Kim, C., Kirkby, J., Kontkanen, J., Kürten, A., Lawler, M. J., Mai, H., Mathot, S., Mauldin, R. L., Molteni, U., Nichman, L., Nie, W., Nieminen, T., Ojdanic, A., Onnela, A., Passananti, M., Petäjä, T., Piel, F., Pospisilova, V., Quéléver, L. L. J., Rissanen, M. P., Rose, C., Sarnela, N., Schallhart, S., Schuchmann, S., Sengupta, K., Simon, M., Sipilä, M., Tauber, C., Tomé, A., Tröstl, J., Väisänen, O., Vogel, A. L., Volkamer, R., Wagner, A. C., Wang, M., Weitz, L., Wimmer, D., Ye, P., Ylisirniö, A., Zha, Q., Carslaw, K. S., Curtius, J., Donahue, N. M., Flagan, R. C., Hansel, A., Riipinen, I., Virtanen, A., Winkler, P. M., Baltensperger, U., Kulmala, M., and Worsnop, D. R.: Multicomponent new particle formation from sulfuric acid, ammonia, and biogenic vapors, Sci. Adv., 4, eaau5363, https://doi.org/10.1126/sciadv.aau5363, 2018.

Li, H., Kupiainen-Määttä, O., Zhang, H., Zhang, X., and Ge, M.: A molecular-scale study on the role of lactic acid in new particle formation: Influence of relative humidity and temperature, Atmos. Environ., 166, 479-487, https://doi.org/10.1016/j.atmosenv.2017.07.039, 2017.

Liu, L., Zhong, J., Vehkamäki, H., Kurtén, T., Du, L., Zhang, X., Francisco, J. S., and Zeng, X. C.: Unexpected quenching effect on new particle formation from the atmospheric reaction of methanol with SO_3, Proc. Natl. Acad. Sci., 116, 24966-24971, https://doi.org/10.1073/pnas.1915459116, 2019.

Liu, L., Yu, F., Tu, K., Yang, Z., and Zhang, X.: Influence of atmospheric conditions on the role of trifluoroacetic acid in atmospheric sulfuric acid-dimethylamine nucleation, Atmos. Chem. Phys., 21, 6221-6230, https://doi.org/10.5194/acp-21-6221-2021, 2021.

Liu, Y., Liu, Y. R., Feng, Y. J., Huang, T., Jiang, S., Wang, Z. H., Cao, H., and Huang, W.: Valine involved sulfuric acid-dimethylamine ternary homogeneous nucleation and its atmospheric implications, Atmos. Environ., 254, 118373, https://doi.org/10.1016/j.atmosenv.2021, 2021b.

Lu, T., and Chen, F.: Multiwfn: A multifunctional wavefunction analyzer, J. Comput. Chem., 33, 580-592, https://doi.org/10.1002/jcc.22885, 2012.

Lu, T., and Chen, Q.: van der Waals potential: an important complement to molecular electrostatic potential in studying intermolecular interactions, Mol. Ecol., 26, 315, https://doi.org/10.1007/s00894-020-04577-0, 2020.

Lu, T., and Chen, Q.: Interaction Region Indicator: A Simple Real Space Function Clearly Revealing Both Chemical Bonds and Weak Interactions, Chem. Methods, 1, 231-239, https://doi.org/10.1002/cmtd.202100007, 2021.

Lu, T.: Visualization Analysis of Covalent and Noncovalent Interactions in Real Space, Angew. Chem. Int. Ed., 64, e202504895, https://doi.org/10.1002/anie.202504895, 2025.

Lu, T.: A comprehensive electron wavefunction analysis toolbox for chemists, Multiwfn, J. Chem. Phys., 161, https://doi.org/10.1063/5.0216272, 2024.

Lu, Y., Yan, C., Fu, Y., Chen, Y., Liu, Y., Yang, G., Wang, Y., Bianchi, F., Chu, B., Zhou, Y., Yin, R., Baalbaki, R., Garmash, O., Deng, C., Wang, W., Liu, Y., Petäjä, T., Kerminen, V. M., Jiang, J., Kulmala, M., and Wang, L.: A proxy for atmospheric daytime gaseous sulfuric acid concentration

https://doi.org/10.5194/egusphere-2026-2831
Preprint. Discussion started: 14 July 2026

in urban Beijing, Atmos. Chem. Phys., 19, 1971-1983, https://doi.org/10.5194/acp-19-1971-2019, 2019.

Ma, F., Su, L., Tang, W., Zhang, R., Zhao, Q., Chen, J., and Xie, H. B.: Sulfuric Acid-Driven Nucleation Enhanced by Amines from Ethanol Gasoline Vehicle Emission: Machine Learning Model and Mechanistic Study, Environ. Sci. Technol., 58, 22278-22287, https://doi.org/10.1021/acs.est.4c06578, 2024.

Mackenzie, R. B., Dewberry, C. T., and Leopold, K. R.: Gas phase observation and microwave spectroscopic characterization of formic sulfuric anhydride, Science, 349, 58-61, https://doi.org/10.1126/science.aaa9704, 2015.

Mallick, S., Kumar, A., and Kumar, P.: Oxidation of HOSO by NH_2: A new path for the formation of an acid rain precursor, Chem. Phys. Lett. 773, 138536, https://doi.org/10.1016/j.cplett.2021.138536, 2021.

Mardirossian, N., and Head-Gordon, M.: How Accurate Are the Minnesota Density Functionals for Noncovalent Interactions, Isomerization Energies, Thermochemistry, and Barrier Heights Involving Molecules Composed of Main-Group Elements?, J. Chem. Theory Comput. 12, 4303-4325, https://doi.org/10.1021/acs.jctc.6b00637, 2016.

McGrath, M. J., Olenius, T., Ortega, I. K., Loukonen, V., Paasonen, P., Kurtén, T., Kulmala, M., and Vehkamäki, H.: Atmospheric Cluster Dynamics Code: a flexible method for solution of the birth-death equations, Atmos. Chem. Phys., 12, 2345-2355, https://doi.org/10.5194/acp-12-2345-2012, 2012.

McMurry, P. H., Fink, M., Sakurai, H., Stolzenburg, M. R., Mauldin III, R. L., Smith, J., Eisele, F., Moore, K., Sjostedt, S., Tanner, D., Huey, L. G., Nowak, J. B., Edgerton, E., and Voisin, D.: A criterion for new particle formation in the sulfur-rich Atlanta atmosphere, J. Geophys. Res. Atmos., 110, https://doi.org/10.1029/2005JD005901, 2005.

Meana-Pañeda, R., Zheng, J., Bao, J. L., Zhang, S., Lynch, B. J., Corchado, J. C., Chuang, Y. Y., Fast, P. L., Hu, W.-P., Liu, Y. P., Lynch, G. C., Nguyen, K. A., Jackels, C. F., Fernández-Ramos, A., Ellingson, B. A., Melissas, V. S., Villà, J., Rossi, I., Coitiño, E. L., Pu, J., Albu, T. V., Zhang, R. M., Xu, X., Ratkiewicz, A., Steckler, R., Garrett, B. C., Isaacson, A. D., and Truhlar, D. G.: Polyrate 2023: A computer program for the calculation of chemical reaction rates for polyatomics. New version announcement, Comput. Phys. Commun., 294, 108933, https://doi.org/10.1016/j.cpc.2023.108933, 2024.

Neese, F.: The ORCA program system, WIREs Comput. Mol. Sci., 2, 73-78, https://doi.org/10.1002/wcms.81, 2012.

Neese, F.: Software update: the ORCA program system, version 4.0, WIREs Comput. Mol. Sci., 8, e1327, https://doi.org/10.1002/wcms.1327, 2018.

Ning, A., Li, J., Du, L., Yang, X., Liu, J., Yang, Z., Zhong, J., Saiz-Lopez, A., Liu, L., Francisco, J. S., and Zhang, X.: Heterogenous Chemistry of I_2O_3 as a Critical Step in Iodine Cycling, J. Am. Chem. Soc., 146, 33229-33238, https://doi.org/10.1021/jacs.4c13060, 2024.

Nolte, C. G., Fraser, M. P., and Cass, G. R.: Gas Phase C2-C10 Organic Acids Concentrations in the Los Angeles Atmosphere, Environ. Sci. Technol., 33, 540-545, https://doi.org/10.1021/es980626d, 1999.

Ortega, I. K., Donahue, N. M., Kurtén, T., Kulmala, M., Focsa, C., and Vehkamäki, H.: Can Highly Oxidized Organics Contribute to Atmospheric New Particle F ormation?, J. Phys. Chem. A, 120, 1452-1458, https://doi.org/10.1021/acs.jpca.5b07427, 2016.

https://doi.org/10.5194/egusphere-2026-2831
Preprint. Discussion started: 14 July 2026

Partanen, L., Vehkamäki, H., Hansen, K., Elm, J., Henschel, H., Kurtén, T., Halonen, R., and Zapadinsky, E.: Effect of Conformers on Free Energies of Atmospheric Complexes, J. Phys. Chem. A, 120, 8613-8624, https://doi.org/10.1021/acs.jpca.6b04452, 2016.

Perri, M. J., Seitzinger, S., and Turpin, B. J.: Secondary organic aerosol production from aqueous photooxidation of glycolaldehyde: Laboratory experiments, Atmos. Environ., 43, 1487-1497, https://doi.org/10.1016/j.atmosenv.2008.11.037, 2009.

Qiao, F., Zhang, R., Zhao, Q., Ma, F., Chen, J., and Xie, H. B.: A Surprisingly High Enhancing Potential of Nitric Acid in Sulfuric Acid-Methylamine Nucleation, Atmosphere, 15, 467, https://doi.org/10.3390/atmos15040467, 2024.

Rong, H., Liu, L., Liu, J., and Zhang, X.: Glyoxylic Sulfuric Anhydride from the Gas-Phase Reaction between Glyoxylic Acid and SO_3: A Potential Nucleation Precursor, J. Phys. Chem. A, 124, 3261-3268, https://doi.org/10.1021/acs.jpca.0c01558, 2020.

Shampine, L. F., and Reichelt, M. W.: The MATLAB ode suite, SIAM J. Sci. Comput., 18, 1-22, https://doi.org/10.1137/s1064827594276424, 1997.

Smith, C. J., Huff, A. K., Ward, R. M., and Leopold, K. R.: Carboxylic sulfuric anhydrides, J. Phys. Chem. A, 124, 601-612, https://doi.org/10.1021/acs.jpca.9b09310, 2020.

Tan, S., Chen, X., and Yin, S.: Comparison results of eight oxygenated organic molecules: Unexpected contribution to new particle formation in the atmosphere, Atmos. Environ., 268, 118817, https://doi.org/10.1016/j.atmosenv.2021.118817, 2022.

Tsona Tchinda, N., Du, L., Liu, L., and Zhang, X.: Pyruvic acid, an efficient catalyst in SO_3 hydrolysis and effective clustering agent in sulfuric-acid-based new particle formation, Atmos. Chem. Phys., 22, 1951-1963, https://doi.org/10.5194/acp-22-1951-2022, 2022.

Walker, M., Harvey, A. J. A., Sen, A., and Dessent, C. E. H.: Performance of M06, M06-2X, and M06-HF Density Functionals for Conformationally Flexible Anionic Clusters: M06 Functionals Perform Better than B3LYP for a Model System with Dispersion and Ionic Hydrogen-Bonding Interactions, J. Phys. Chem. A, 117, 12590-12600, https://doi.org/10.1021/jp408166m, 2013.

Wang, M., Xiao, M., Bertozzi, B., Marie, G., Rörup, B., Schulze, B., Bardakov, R., He, X. C., Shen, J., Scholz, W., Marten, R., Dada, L., Baalbaki, R., Lopez, B., Lamkaddam, H., Manninen, H. E., Amorim, A., Ataei, F., Bogert, P., Brasseur, Z., Caudillo, L., De Menezes, L.-P., Duplissy, J., Ekman, A. M. L., Finkenzeller, H., Carracedo, L. G., Granzin, M., Guida, R., Heinritzi, M., Hofbauer, V., Höhler, K., Korhonen, K., Krechmer, J. E., Kürten, A., Lehtipalo, K., Mahfouz, N. G. A., Makhmutov, V., Massabò, D., Mathot, S., Mauldin, R. L., Mentler, B., Müller, T., Onnela, A., Petäjä, T., Philippov, M., Piedehierro, A. A., Pozzer, A., Ranjithkumar, A., Schervish, M., Schobesberger, S., Simon, M., Stozhkov, Y., Tomé, A., Umo, N. S., Vogel, F., Wagner, R., Wang, D. S., Weber, S. K., Welti, A., Wu, Y., Zauner-Wieczorek, M., Sipilä, M., Winkler, P. M., Hansel, A., Baltensperger, U., Kulmala, M., Flagan, R. C., Curtius, J., Riipinen, I., Gordon, H., Lelieveld, J., El-Haddad, I., Volkamer, R., Worsnop, D. R., Christoudias, T., Kirkby, J., Möhler, O., and Donahue, N. M.: Synergistic HNO_3-H_2SO_4-NH_3 upper tropospheric particle formation, Nature, 605, 483-489, https://doi.org/10.1038/s41586-022-04605-4, 2022.

Wang, R., Li, R., Chen, S., Mu, R., Zhang, C., Ma, X., Khan, M., and Zhang, T.: Enhancing SO_3 hydrolysis and nucleation: the role of formic sulfuric anhydride, Atmos. Chem. Phys., 25, 5695-5709, https://doi.org/10.5194/acp-25-5695-2025, 2025.

Xie, H. B., Elm, J., Halonen, R., Myllys, N., Kurtén, T., Kulmala, M., and Vehkamäki, H.: Atmospheric Fate of Monoethanolamine: Enhancing New Particle Formation of Sulfuric Acid as an Important

https://doi.org/10.5194/egusphere-2026-2831
Preprint. Discussion started: 14 July 2026

Removal Process, Environ. Sci. Technol., 51, 8422-8431, https://doi.org/10.1021/acs.est.7b02294, 2017.

Yang, L., Nie, W., Liu, Y., Xu, Z., Xiao, M., Qi, X., Li, Y., Wang, R., Zou, J., Paasonen, P., Yan, C., Xu, Z., Wang, J., Zhou, C., Yuan, J., Sun, J., Chi, X., Kerminen, V. M., Kulmala, M., and Ding, A.: Toward Building a Physical Proxy for Gas-Phase Sulfuric Acid Concentration Based on Its Budget Analysis in Polluted Yangtze River Delta, East China, Environ. Sci. Technol., 55, 6665-6676, https://doi.org/10.1021/acs.est.1c00738, 2021.

Yao, L., Garmash, O., Bianchi, F., Zheng, J., Yan, C., Kontkanen, J., Junninen, H., Mazon, S. B., Ehn, M., Paasonen, P., Sipilä, M., Wang, M., Wang, X., Xiao, S., Chen, H., Lu, Y., Zhang, B., Wang, D., Fu, Q., Geng, F., Li, L., Wang, H., Qiao, L., Yang, X., Chen, J., Kerminen, V. M., Petäjä, T., Worsnop, D. R., Kulmala, M., and Wang, L.: Atmospheric new particle formation from sulfuric acid and amines in a Chinese megacity, Science, 361, 278-281, https://doi.org/10.1126/science.aao4839, 2018.

Zhang, H., Kupiainen-Määttä, O., Zhang, X., Molinero, V., Zhang, Y., and Li, Z. J. T. J. o. C. P.: The enhancement mechanism of glycolic acid on the formation of atmospheric sulfuric acid-ammonia molecular clusters, J. Chem. Phys. 146, https://doi.org/10.1021/acs.est.1c00738,2017.

Zhang, H., Wang, W., Pi, S., Liu, L., Li, H., Chen, Y., Zhang, Y., Zhang, X., and Li, Z.: Gas phase transformation from organic acid to organic sulfuric anhydride: Possibility and atmospheric fate in the initial new particle formation, Chemosphere, 212, 504-512, https://doi.org/10.1016/j.chemosphere.2018.08.074, 2018.

Zhang, H., Wang, W., Li, H., Gao, R., and Xu, Y.: A theoretical study on the formation mechanism of carboxylic sulfuric anhydride and its potential role in new particle formation, RSC Adv., 12, 5501-5508, https://doi.org/10.1039/D2RA00226D, 2022.

Zhang, H., Gao, R., Li, H., Li, Y., Xu, Y., and Chai, F.: Formation mechanism of typical aromatic sulfuric anhydrides and their potential role in atmospheric nucleation process, J. Environ. Sci., 123, 54-64, https://doi.org/10.1016/j.jes.2022.01.015, 2023.

Zhang, J., and Dolg, M.: ABCluster: the artificial bee colony algorithm for cluster global optimization, Phys. Chem. Chem. Phys., 17, 24173-24181, https://doi.org/10.1039/C5CP04060D, 2015.

Zhang, R., Khalizov, A., Wang, L., Hu, M., and Xu, W.: Nucleation and Growth of Nanoparticles in the Atmosphere, Chem. Rev., 112, 1957-2011, https://doi.org/10.1021/cr2001756, 2012.

Zhang, R., Wang, G., Guo, S., Zamora, M. L., Ying, Q., Lin, Y., Wang, W., Hu, M., and Wang, Y.: Formation of Urban Fine Particulate Matter, Chem. Rev., 115, 3803-3855, https://doi.org/10.1021/acs.chemrev.5b00067, 2015.

Zhang, Z. P., Wang, S. H., Shang, Y. L., Liu, J. H., and Luo, S. N.: Theoretical Study on Ethylamine Dissociation Reactions Using VRC-VTST and SS-QRRK Methods, J. Phys. Chem. A, 128, 2191-2199, https://doi.org/10.1021/acs.jpca.3c08373, 2024.

Zhao, B., Donahue, N. M., Zhang, K., Mao, L., Shrivastava, M., Ma, P.-L., Shen, J., Wang, S., Sun, J., Gordon, H., Tang, S., Fast, J., Wang, M., Gao, Y., Yan, C., Singh, B., Li, Z., Huang, L., Lou, S., Lin, G., Wang, H., Jiang, J., Ding, A., Nie, W., Qi, X., Chi, X., and Wang, L.: Global variability in atmospheric new particle formation mechanisms, Nature, 631, 98-105, https://doi.org/10.1038/s41586-024-07547-1, 2024.

Zhao, J., Smith, J. N., Eisele, F. L., Chen, M., Kuang, C., and McMurry, P. H.: Observation of neutral sulfuric acid-amine containing clusters in laboratory and ambient measurements, Atmos. Chem. Phys., 11, 10823-10836, https://doi.org/10.5194/acp-11-10823-2011, 2011.

https://doi.org/10.5194/egusphere-2026-2831
Preprint. Discussion started: 14 July 2026

712 Zhao, Y., and Truhlar, D. G.: The M06 suite of density functionals for main group thermochemistry,
713 thermochemical kinetics, noncovalent interactions, excited states, and transition elements: two new
714 functionals and systematic testing of four M06-class functionals and 12 other functionals, Theor.
715 Chem. Acc., 120, 215-241, https://doi.org/10.1007/s00214-007-0310-x, 2008.
716 Zheng, J., Ma, Y., Chen, M., Zhang, Q., Wang, L., Khalizov, A. F., Yao, L., Wang, Z., Wang, X., and
717 Chen, L.: Measurement of atmospheric amines and ammonia using the high resolution time-of-
718 flight chemical ionization mass spectrometry, Atmos. Environ., 102, 249-259,
719 https://doi.org/10.1016/j.atmosenv.2014.12.002, 2015.
720

https://doi.org/10.5194/egusphere-2026-2831
Preprint. Discussion started: 14 July 2026

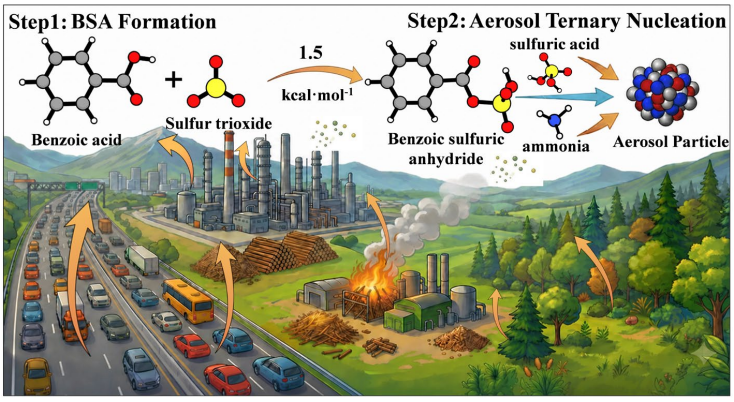

Graphic abstract

https://doi.org/10.5194/egusphere-2026-2831
Preprint. Discussion started: 14 July 2026

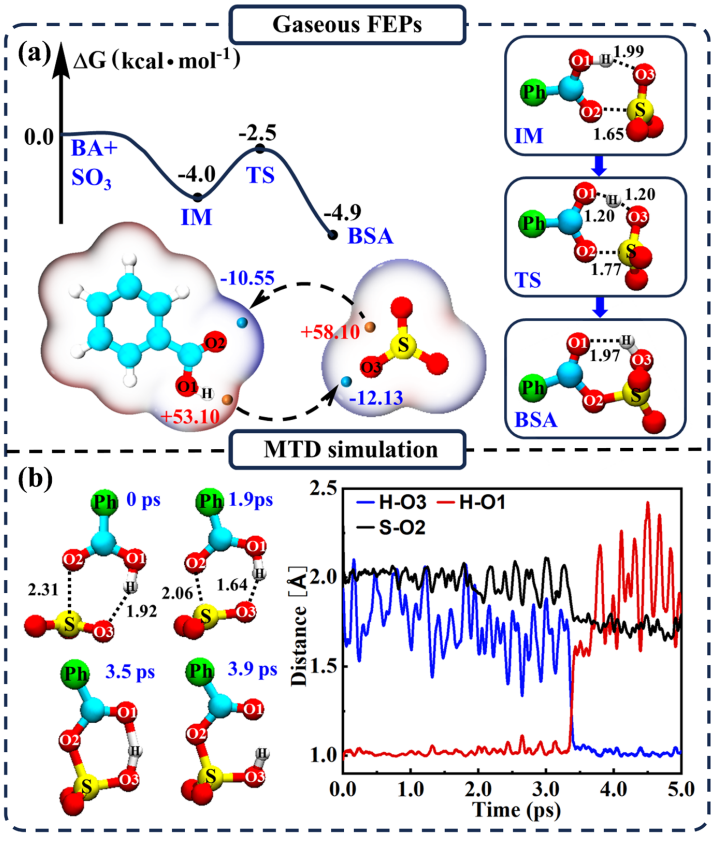

Fig. 1. (a) Schematic potential energy surface for the reaction of BA with SO_3 at the DLPNO-CCSD(T)/aug-cc-pVTZ//M06-2X/6-311G(2*d*,2*p*) level and computed electrostatic potential-mapped molecular van der Waals (vdW) surfaces of BA interacting with SO_3 at the M06-2X/6-311G(2*d*,2*p*) level; (b) MTD trajectories depicting the reaction dynamics of BA + SO_3 in the gas phase.

https://doi.org/10.5194/egusphere-2026-2831
Preprint. Discussion started: 14 July 2026

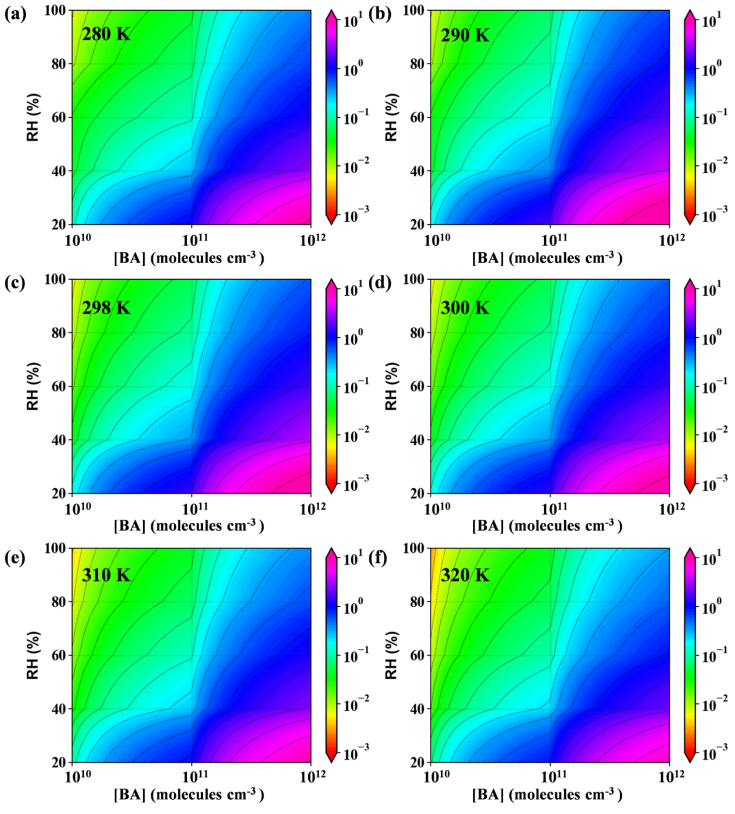

731

732 **Fig. 2.** Rate ratios of ν_{BA}/ν_{SA_wm} (280-320 K) under different atmospheric conditions: (i) H_2O
733 concentrations corresponding to 20-100% relative humidity (RH); (ii) BA concentrations ranging
734 from 10^{10} to 10^{12} molecules·cm^{-3}.

735

https://doi.org/10.5194/egusphere-2026-2831
Preprint. Discussion started: 14 July 2026

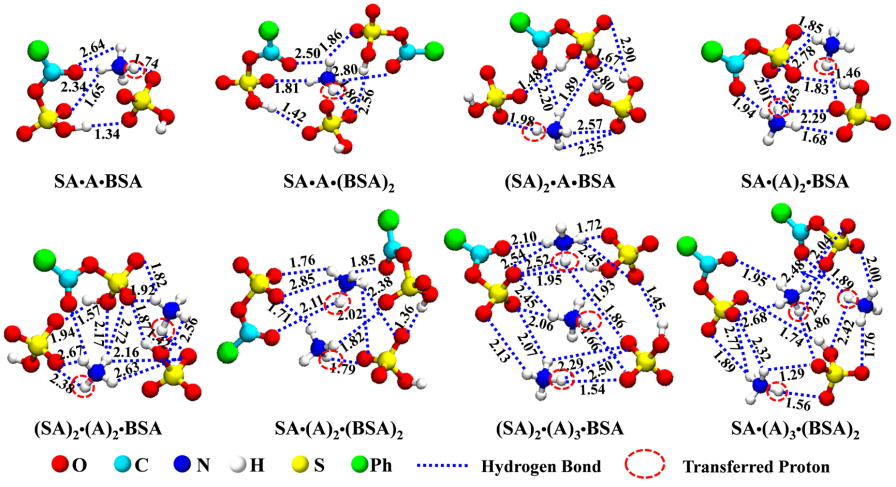

Fig. 3. The lowest free energy configurations of representative BSA-SA-A clusters. The blue dashed lines indicate hydrogen bonds, while red dashed circles denote transferred protons. Black numbers represent hydrogen-bond lengths, and all bond lengths are given in Å.

https://doi.org/10.5194/egusphere-2026-2831
Preprint. Discussion started: 14 July 2026

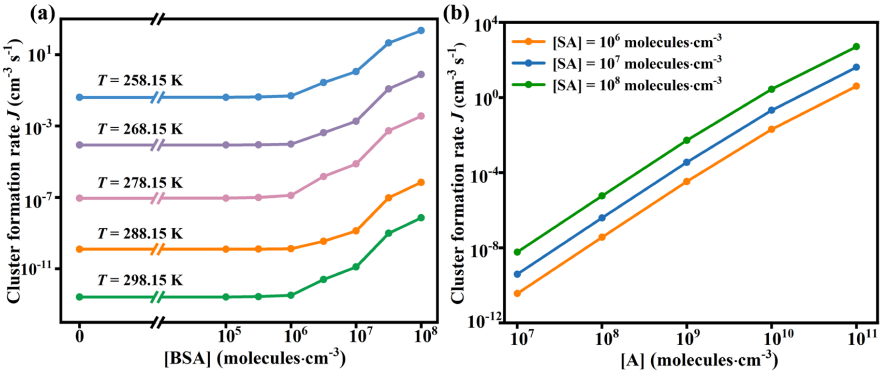

741

742 **Fig. 4** The cluster formation rates J (cm^{-3} s^{-1}) of the BSA-SA-A system. (a) as a function of BSA as
743 a function of [BSA] from 10^5 to 10^8 molecules·cm^{-3} under different temperatures where [SA] = 10^7
744 molecules·cm^{-3} and [A] = 10^9 molecules·cm^{-3} (b) as a function of [A] with [BSA] = 10^8
745 molecules·cm^{-3} and under three different [SA] at 278.15 K.

746

https://doi.org/10.5194/egusphere-2026-2831
Preprint. Discussion started: 14 July 2026

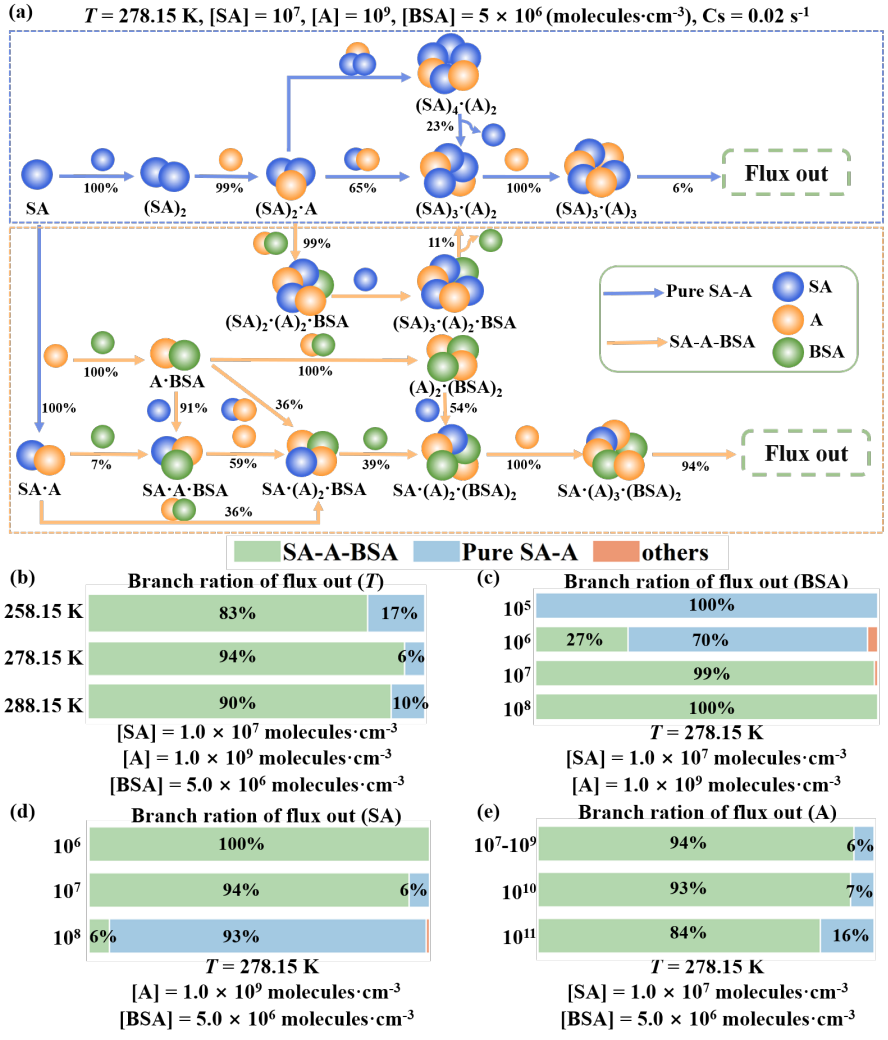

Fig. 5 Nucleation mechanism of the BSA-SA-A system. (a) cluster growth pathways of the BSA-SA-A nucleation systems at 278.15 K, under conditions of CS = 0.02 s^{-1}, [SA] = 10^7 molecules·cm^{-3}, [A] = 10^9 molecules·cm^{-3} and [BSA] = 5 × 10^6 molecules·cm^{-3}. The blue and orange arrows represent the growth pathways of the pure SA-A clusters and BSA-containing SA-A-BSA clusters, respectively. Relative contributions of the pure SA-A pathway and the BSA-involved pathway to the total flux out of the system as functions of (b) temperature (c) [BSA] (d) [SA] and (e) [A].

https://doi.org/10.5194/egusphere-2026-2831
Preprint. Discussion started: 14 July 2026

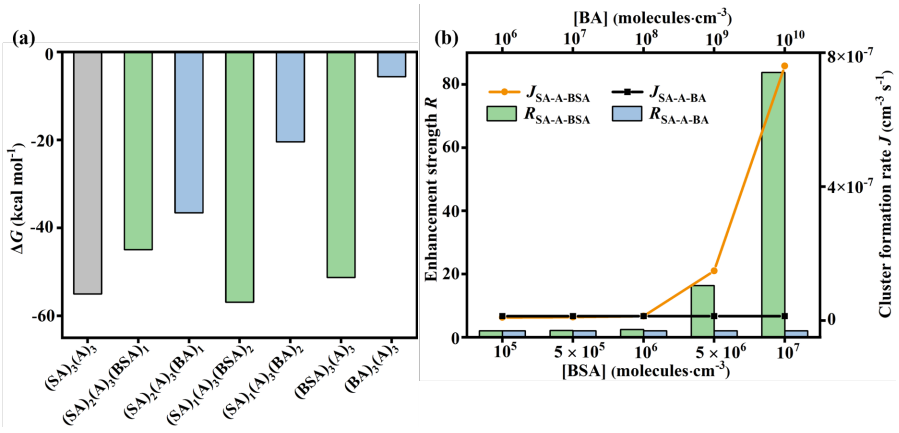

Fig. 6 Comparison of the effects of BSA and BA on SA-A system. (a) Gibbs free energies ΔG (kcal·mol^{-1}) for $(BSA)_x(SA)_y(A)_3$ and $(BA)_x(SA)_y(A)_3$ (x = 0-3, and $x + y = 3$) clusters calculated at 278.15 K; (b) Cluster formation rate (J) and enhancement strength (R) for BSA as a function of monomer concentrations [BSA]and [BA])) at 278.15 K, with [SA] fixed at 10^7 molecules·cm^{-3} and [A] at 10^9 molecules·cm^{-3}.